http://dx.doi.org/10.5012/bkcs.2014.35.1.151

Coriolis Coupling Influence on the H+LiH Reaction

Hongsheng Zhai, Wenliang Li,† and Yufang Liu*

*Department of Physics, Henan Normal University, Xinxiang 453007, China. *E-mail: yf-liu@henannu.edu.cn*
Key Laboratory at Universities of Education, Department of Xinjiang Uygur Autonomous Region for New Energy Materials, Xinjiang Institute of Engi-neering, Urumqi, Xinjiang 830091, China
Received September 5, 2013, Accepted October 16, 2013

We have reported the reaction probability, integral reaction cross section, and rate constant for the title system calculated with the aid of a time-dependent wave packet approach. The *ab initio* potential energy surface (PES) of Prudente *et al*. (*Chem. Phys. Lett.* **2009**, *474*, 18) is employed for the purpose. The calculations are carried out over the collision energy range of 0.05-1.4 eV for the two reaction channels of H + LiH → Li + H_2 and H_b + LiH_a → LiH_b + H_a. The Coriolis coupling (CC) effect are taken into account. The importance of including the Coriolis coupling quantum scattering calculations are revealed by the comparison between the Coriolis coupling and the centrifugal sudden (CS) approximation calculations.

Key Words : Reaction probability, Integral cross section, Rate constant, Quantum wave-packet

Introduction

The formation and depletion of LiH and its ionic species were believed to play rather important role in the stellar evolution and galactic lithium production.[1-6] Many experimental and theoretical studies about the formation and depletion reaction of LiH and its ionic variants were reported.[2,3,6-8] Bililign *et al*.[9] conducted laser induced pump-probe far-wing scattering experiments to study the photochemical reaction Li + H_2 → LiH + H. Chen *et al*.[10] observed the nascent rotational population distribution of LiH in the atom Li plus diatom molecule H_2 reaction by using a pump-probe technique. The comprehensive chemistry of lithium in the post-recombination epoch is presented by Stancil *et al*.[3] and the abundances of Li, Li^+, Li^-, LiH and LiH^+ were employed for calculation as a function of red-shift z for several cosmological models. Theoretical studies on the spectroscopic, polarizability and mono-bichromatic electron dynamics of the LiH have been reported.[11-14]

The LiH_2 chemical system has been the subject of a large number of studies on its potential energy surfaces (PESs), on the sub-reactive or reactive collision dynamics during the past decade.[15-28] The ground state potential energy surface (PES) of LiH_2 system for the collinear arrangement was initially constructed by Clarke *et al*.[16] and also for the three-dimensional configurations by Dunne, Murrell, and Jemmer (DMJ PES).[18] Clarke and coworkers[16] have calculated the initial state selected reaction probabilities for the depletion and formation reaction of LiH by the quasi-classical trajectory (QCT) and the quantum time-dependent wave packet method for the special collinear arrangement. The dynamical results indicated the depletion reaction is strongly exothermic and appears to be a direct reaction without any transition state region. Dunne *et al*.[18] have studied the temperature dependence of the rate of the depletion reaction and provided with a satisfactory analytical fit to this rate. The Kim and coworkers[22] have performed QCT calculations on the resulting interpolated PES. Their findings indicated a direct nature of the reaction H + LiH → Li + H_2, and the internal energy of the reagent LiH does influence the reaction dynamics. Padmanaban *et al*.[19,20] have carried out an intensive investigation for the hydrogen exchange channel and the HLi depletion channel with the aid of a time-dependent wave-packet approach on the DMJ PES. The initial-state-selected and energy-resolved total reaction probabilities, initial state-selected reaction cross sections and temperature-dependent rate constants were calculated.

In order to gets rid of the unphysical well on the DMJ PES, Wernli *et al*.[28] present a new three dimensional PES for the electronic ground state reaction LiH + H and Prudente *et al*.[15] reported an accurate potential energy surface (here we call PMM PES) for the ground electronic state of LiH_2 system which improved the DMJ PES by FCI/aug-cc-pVQZ *ab* initio calculation. It is worth noting that the reaction probability for the formation of Li+H_2 is higher than the result of the H-exchange channel on the PMM PES, while the reverse pattern was found with the DMJ PES.

There are two reaction channel in the title reaction, the exothermic reaction H + LiH → Li + H_2 which is considered to contribute to LiH depletion, and the thermoneutral H-exchange reaction H_b + LiH_a → LiH_b + H_a. In this paper, we focus on the the dynamics of H+LiH collision in these two reaction channels based on the PMM PES reported by Prudente *et al*.[15] Detailed calculations of the title reaction are presented with the aid of quantum wave packet method. As is known, the Coriolis coupling effect plays an important role in many geophysical/astrophysical fluid-dynamical systems and polyatomic systems. In order to analyze the role of Coriolis coupling effect in title reactive chemical processes, the centrifugal sudden (CS) approximation is employed in the dynamics calculations.

Theoretical Method

The Schrodinger equation that is to be numerically solved in a reactive scattering calculation for a triatomic A+BC reaction is written as:

$$i\hbar\frac{\partial}{\partial t}\psi = \hat{H}\psi \tag{1}$$

Using the reactant Jacobi coordinates, the Hamiltonian operator for a triatomic system is given by,

$$\hat{H} = \frac{\hbar^2}{2\mu_R}\frac{\partial^2}{\partial R^2} - \frac{\hbar^2}{2\mu_r}\frac{\partial^2}{\partial r^2} + V(R,r) + \frac{\hat{L}^2}{2\mu_R R^2} + \frac{\hat{j}^2}{2\mu_r r^2} \tag{2}$$

here, R is the distance between atom A and the center-of-mass of molecule BC, r the diatomic distance, μ_R and μ_r the corresponding reduced masses. $\hat{j}$ is the diatomic rotational angular momentum operator, $\hat{L}^2$ the orbital angular momentum operator, and $V(R,r)$ the adiabatic potential energy surface. The quantum calculation is carried out using the time-dependent wave packet method developed by Zhang.[29]

In the time-dependent wave packet method, the Schrodinger Eqn. (1) is solved by propagating the wave function with a split-operator scheme,

$$\psi(t+\Delta) = e^{-iH_0\Delta/2}e^{-iV_{\rm rot}\Delta/2}e^{-iV\Delta/2}e^{-iV_{\rm rot}\Delta/2}e^{-iH_0\Delta/2}\psi \tag{3}$$

With $\hat{H}_0=\frac{\hbar^2}{2\mu_R}\frac{\partial^2}{\partial R^2} - \frac{\hbar^2}{2\mu_R}\frac{\partial^2}{\partial r^2}+V(r)$ and $\hat{V}_{\rm rot}=\frac{\hat{L}^2}{2\mu_R R^2}+\frac{\hat{j}^2}{2\mu_r r^2}$

t is the propagation time and Δ the time interval, and V is the adiabatic potential energy surface. $V(r)$ in Eqn. (4) is the diatomic reference potential.

The following formulae[30-35] are used to extract the initial state (j_0, k_0, k_0) resolved total reaction probabilities and the integral cross sections after the wave packet is propagated for a sufficiently long time,

$$P^J_{j_0k_0v_0} = \sum_j \frac{\hbar}{\mu_r}\mathrm{Im}[\langle\psi(E)|\delta(s-s_0)|\psi(E)\rangle] \tag{4}$$

$$\sigma_{j_0k_0v_0}(E) = \frac{\pi}{k^2}\sum_j (2J+1)P^J_{j_0k_0v_0}(E) \tag{5}$$

$$\sigma_{j_0v_0}(E) = \frac{1}{2j_0+1}\sum_{k_0}\sigma_{j_0k_0v_0}(E) \tag{6}$$

$\psi(E)$ is the corresponding time-independent part of the wave function $\psi(t)$, s_0 represents the position where the flux calculation is carried out along the R or r directions (s_0 = R or r). Table 1 listed the parameters used in this quantum scattering calculations to obtain the converged reaction probabilities. For more details about the quantum method, the readers are referred to Ref.[30-35]

The thermal rate constant is calculated from the total reaction cross section using the expression:

$$k(T) = \eta\sqrt{\frac{k_BT}{\pi\mu_R}}(k_BT)^{-2}\int_0^\infty E\sigma(E)\exp\left(-\frac{E}{k_BT}\right)dE \tag{7}$$

where μ_R is the reduced mass of H+Li, and k_B is the Boltzmann constant.

The quantum calculation is carried out on the adiabatic ground potential energy surface in the body-fixed (BF) frame and the wave function is expanded within a translational–vibrational–BF rotational basis set $|n|v|J\Omega j\Omega\rangle$, $|n\rangle$ and $|v\rangle$ express the translational and vibrational basis functions, respectively, $|J\Omega j\Omega\rangle$ represents the BF rotational basis function and describes the angular motion with Ω being the projection of total angular momentum J and j onto the BF z axis. Based on this, the element of the Hamiltonian matrix is expressed as

$$\begin{aligned}H_{n'v'j'\Omega',nvj\Omega} &= \langle n'|-\frac{\hbar^2}{2\mu_R}\frac{\partial^2}{\partial R^2}|n\rangle\delta_{vv'}\delta_{jj'}\delta_{\Omega\Omega'}\\ &+ \langle v'|-\frac{\hbar^2}{2\mu_R}\frac{\partial^2}{\partial R^2}|v\rangle\delta_{vv'}\delta_{jj'}\delta_{\Omega\Omega'}\\ &+ \langle n'|\langle v'|\langle J\Omega'j'\Omega'|V(\hat{R},\hat{r})|J\Omega j\Omega\rangle|v\rangle|n\rangle\\ &+ \langle v'|\langle J\Omega'j'\Omega'|\frac{\hat{j}^2}{2\mu_r r^2}|J\Omega j\Omega\rangle|v\rangle\delta_{nn'}\\ &+ \langle n'|\langle J\Omega'j'\Omega'|\frac{\hat{L}^2}{2\mu_R R^2}|J\Omega j\Omega\rangle|n\rangle\delta_{vv'}\end{aligned} \tag{8}$$

Coriolis coupling terms are "buried" in the fifth centrifugal term $\hat{L}^2/2\mu_R R^2$, by substituting $\hat{L} = \hat{j}-\hat{j}$ in the centrifugal term and by using a rotational basis of associated Legendre polynomials,

$$\begin{aligned}&\langle J\Omega'j'\Omega'|\hat{L}^2|J\Omega j\Omega\rangle = \langle J\Omega'j'\Omega'|(\hat{j}-\hat{j})^2|J\Omega j\Omega\rangle\\ &= [J(J+1)+j(j+1)-2\Omega^2]\delta_{jj'}\delta_{\Omega\Omega'} - [J(J+1)\\ &- \Omega(\Omega+1)]^{1/2}[j(j+1)-\Omega(\Omega+1)]^{1/2}\delta_{jj'}\delta_{\Omega'\Omega+1}\\ &- [J(J+1)-\Omega(\Omega-1)]^{1/2}[j(j+1)-\Omega(\Omega-1)]^{1/2}\delta_{jj'}\delta_{\Omega'\Omega-1}\end{aligned} \tag{9}$$

We can see here that the Hamiltonian is block-tridiagonal in Ω. In other words, the Ω substates are coupled through the orbital angular momentum, and such Ω coupling defines the rotational Coriolis coupling in adiabatic quantum dynamics, which constitutes the off-diagonal element of Coriolis coupling matrix given by Eqn. (9).

In the CS approximation, the off-diagonal elements (Ω couplings) are neglected, leading to a simplified expression of Eqn. (9)

$$\langle J\Omega'j'\Omega'|\hat{L}^2|J\Omega j\Omega\rangle = [J(J+1)+j(j+1)-2\Omega^2]\delta_{jj'}\delta_{\Omega\Omega'} \tag{10}$$

Consequently, the size of the Coriolis matrix is reduced due to the neglect of the off-diagonal Coriolis couplings.

Results and Discussion

In this work, we have employed the Coriolis coupling (CC) and centrifugal sudden (CS) approximation calculations, respectively.[34] To get the converged results, the number of K

Table 1. Parameters for the quantum calculations (all quantities are given in a.u., unless otherwise indicated)

Scattering coordinate (R) range	0.2–25.0
Number of grid points in R	300(200)
Internal coordinate (r) range	0.5–17.0
Number of vibrational basis functions	140
Number of rotational basis functions	100
Absorption region length in R (r)	3 (3)
Absorption strength in R (r)	0.03 (0.03)
Center of initial wavepacket (R_0)	18.0
Initial translational energy (eV)	0.65
Analysis line	12.0
Propagation time	30 000

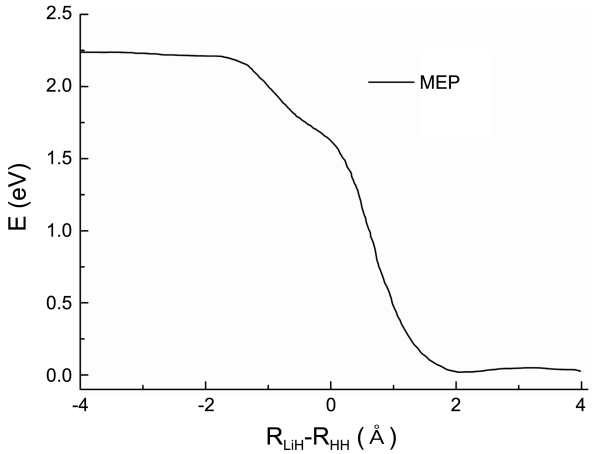

Figure 1. Reaction profile along the absolute minimum energy path (MEP) from the Ref. 15.

used in the CC calculations is up to 3, where K is the projection of J on the space fixed and body-fixed z axis. The reaction cross sections were calculated using all J values in the range of $0 \le J \le J_{max}$. In the CS and CC calculations, J_{max} was about 80 to converge the cross section in the investigated energy range.

The comparison between the CS and CC probabilities as a function of the collision energy for the H+LiH(v, j) reaction are presented in Figures 2 and 3. Where, Figure 2 shows the probability of the LiH depletion channel and the Figure 3 expresses that of the H-exchange channel. The vibrational and rotational quantum number (v, j) of the diatom LiH are set to be zero. It is noticeable that the probabilities of the LiH depletion channel are larger than those of the H-exchange channel. When the J reaches to about 50, the probabilities of the H-exchange channel are close to zero. This will be shown easily in the following integral reaction cross section calculations. In Figure 2, the LiH depletion channel probability of CC calculation is larger than the CS result when

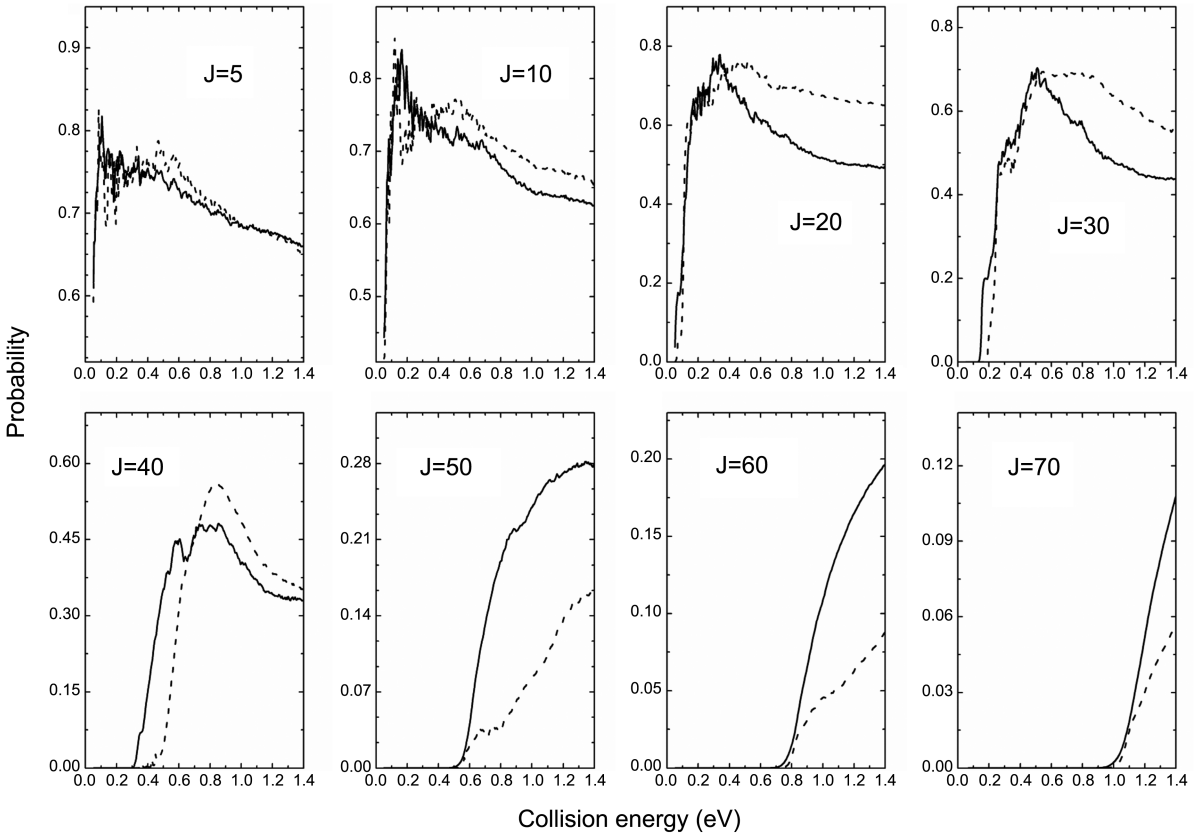

Figure 2. The comparison between the CS and CC probabilities for the HLi depletion channel in the collision energy range of 0-1.0 eV for initial quantum numbers v = 0, j = 0 and for total angular momenta J = 5, J = 10, J = 20, J = 30, J = 40, J = 50, J = 60, J = 70. The solid lines are the CC results and the dash lines express the CS calculation.

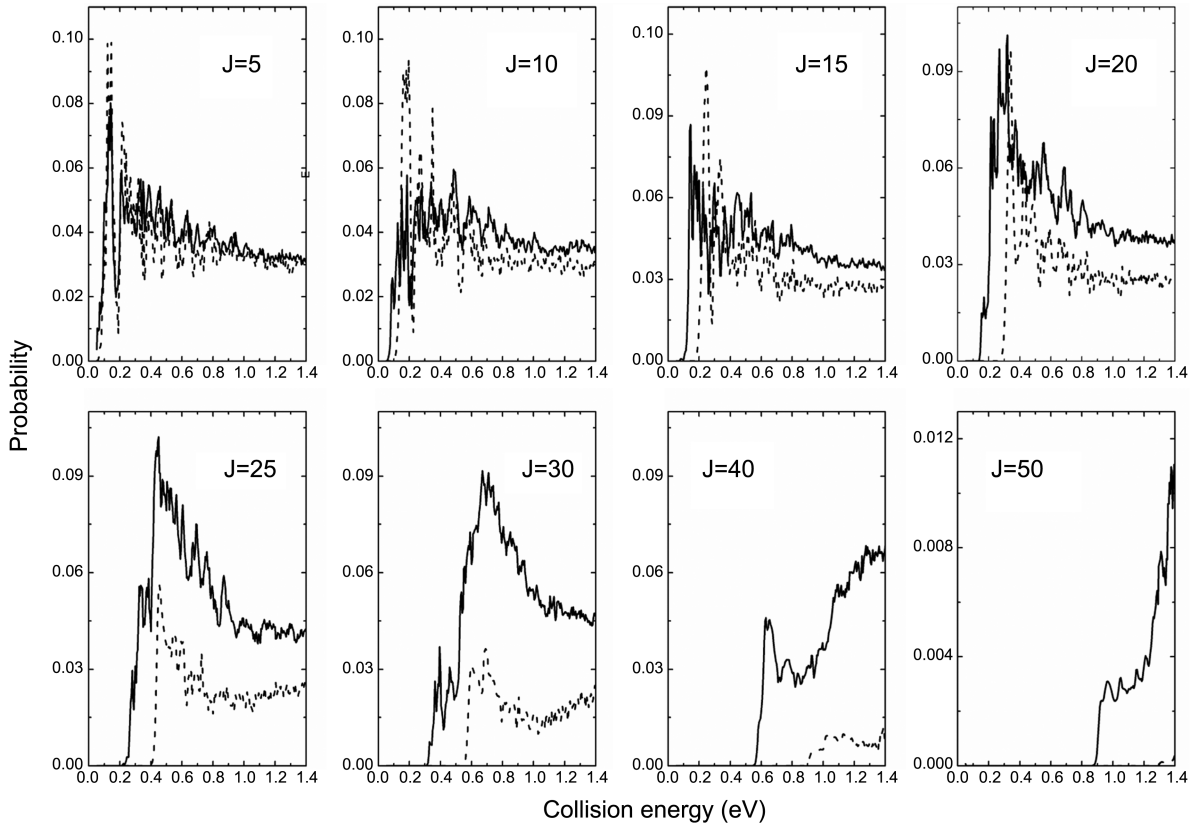

Figure 3. The comparison between the CS and CC probabilities for the H-exchange channel in the collision energy range of 0-1.0 eV for initial quantum numbers $v = 0$, $j = 0$ and for total angular momenta $J = 5$, $J = 10$, $J = 15$, $J = 20$, $J = 25$, $J = 30$, $J = 40$, $J = 50$. The solid lines are the CC results and the dash lines express the CS calculations.

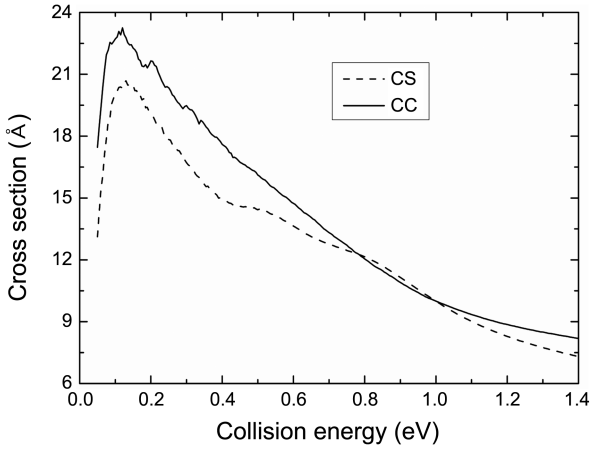

Figure 4. The integral cross sections as a function of collision energy from 0.05 to 1.4 eV for the LiH depletion channel in the reaction H+LiH. The solid line denotes the CC result. The dash line indicates the CS calculation.

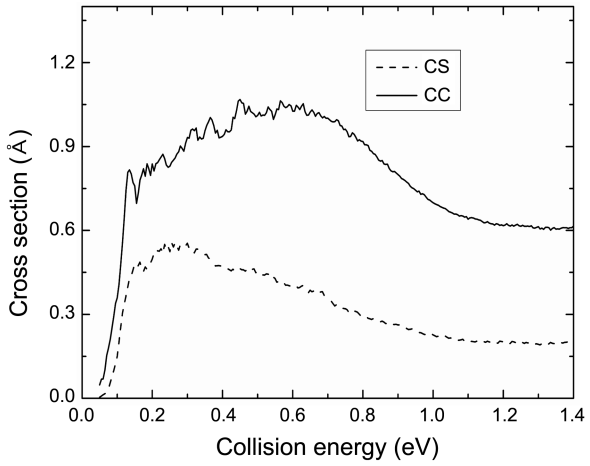

Figure 5. The integral cross sections as a function of collision energy from 0.05 to 1.4 eV for the H-exchange channel in the reaction H+LiH. The solid line denotes the CC result. The dash line indicates the CS calculation.

the collision energy bellows 0.4 eV. The CC probability is lower than the CS calculation at the J range of 10-40 above the collision energy 0.4 eV and the inverse trend is presented when the J is from 40 to 80. For the H-exchange channel, the CC probability is always larger than the CS result and the difference become large with the increasing J.

Figures 4 and 5 illustrate the CC and CS integral cross sections of the two channels as a function of collision energy for the reaction H + LiH ($v = 0$, $j = 0$). The cross sections for the LiH depletion channel is evidently large than the H-exchange channel results. It indicates that the LiH depletion channel is predominant in the title reaction. In Figure 1, the minimum energy path on PES shows a purely downhill route to the product and there is a shallow well in the exit channel. According to the theory of the reaction $H+LiH^+$ of Ref. 23,

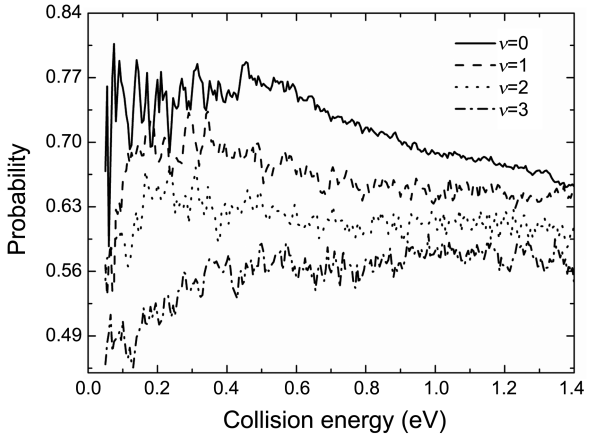

Figure 6. The reaction probabilities of H + LiH (v = 0-3, j = 0) → Li + H_2 for J = 0 as a function of the collision energy.

the potential well is too shallow to allow formation of an long-lived collision complexes, thus a direct dynamics should take place. From the comparison between the CC and CS cross sections for the LiH depletion channel in Figure 4, we can see the CC result is larger than the CS one and the difference tends to diminish at high collision energy. It illustrates that the Coriolis coupling effect is insignificant at low collision energy. As shown in Figure 5, the CC calculation is above the CS result and the tendency of difference between the CC and CS increases with increasing collision energy. The difference between CC and CS results of the H-exchange channel is distinctly greater than that of the LiH depletion channel. Obviously, the Coriolis coupling effect in the H-exchange channel is more effectively than that in the LiH depletion channel. It indicates that the reaction is mainly dominated by the direct reaction mechanism, the insertion reaction mechanism play a role when the collision energy is low.

The CC probabilities obtained with the vibrational excited reagent LiH (v = 0-3, j = 0) are plotted in Figures 6 and 7. The channel 1 expresses the LiH depletion reaction and the channel 2 represents the H-exchange reaction. It can be seen that the CC value for a given energy decreases with increasing vibrational quantum number for the LiH depletion channel, but the opposite change occurs in the H-exchange channel. It indicates that the reaction is inclined to the H-exchange channel as the vibrational excitation increases.

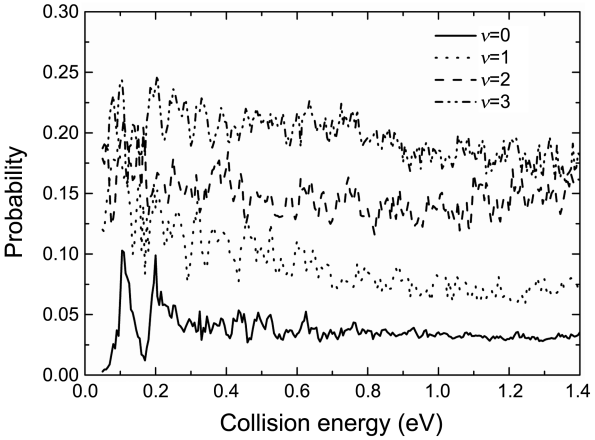

Figure 7. The reaction probabilities of H_b + LiH_a (v = 0-3, j = 0) → LiH_b + H_a for J = 0 as a function of the collision energy.

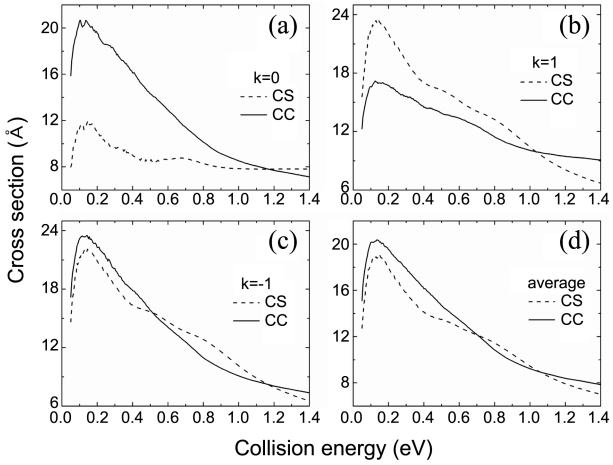

Figure 8. A comparison between the CC and CS cross section in the collision energy range of 0.05-1.4 eV for for j = 1; v = 0; k = 0, 1, −1 and k averged in the LiH depletion channel.

Figure 8 shows the CC and CS cross sections $\sigma_{j_0k_0v_0}$ (v = 0; j = 1; k = 0, ± 1) and $\sigma_{j_0k_0v_0}$ (v = 0; j = 1) with averaging over k as a function of collision energy in the LiH depletion channel. The CS cross sections with k = 0 and k = −1 are smaller than the corresponding CC results in the low energy regions, while the difference between CC and CS results dwindle with the increasing collision energy and the CC cross sections are larger than the CS ones at the high collision energy. The inverse situation is presented in Figure 8(b) with k = 1. The CC and CS total reaction cross sections with averaging over k for j = 1 and v = 0 in Figure 8(d) is similar to the sections for j = 0 and v = 0 but lower than the latter results. The CC and CS cross sections in the H-exchange channel are presented in Figure 8. The difference between the CC and CS with k = 0 and k = −1 are small in

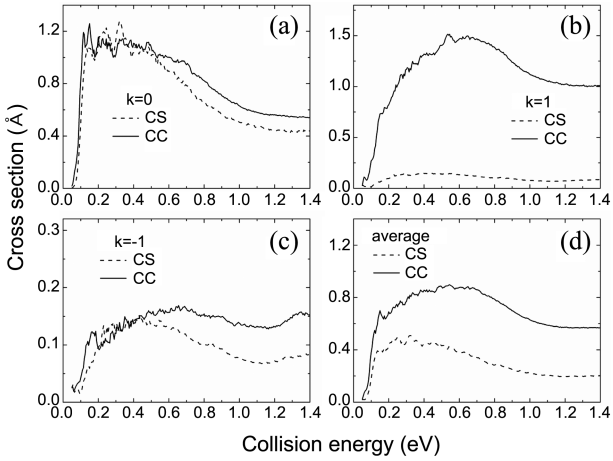

Figure 9. A comparison between the CC and CS cross section in the collision energy range of 0.05-1.4 eV for j = 1; v = 0; k = 0, 1, −1 and k averged in the H-exchange channel.

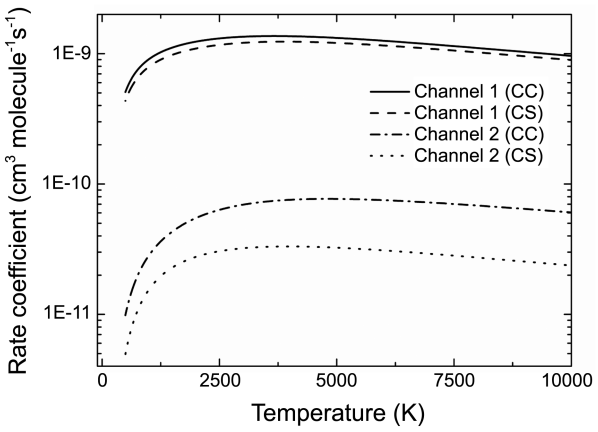

Figure 10. The thermal rate constants as a function of temperature over the range of 400 K to 10000 K. The solid line and dash line denote the CC and CS calculations of the exothermic reaction channel (channel 1), the dish dot line and dot line are the CC and CS results of the H-exchange reaction channel (channel 2).

the low energy regions and rise with the increasing collision energy. Noticeably, the CC calculation is greatly larger than CS result in Figure 9(b) with $k = 1$. Due to the contribution of the result for $k = 1$, the CC section with averaging over k is larger than the CS one. As a whole, the total cross sections for ($j = 1$, $v = 0$) are smaller than that for ($j = 0$, $v = 0$) in the two reaction channels, it indicates that the high rotational excitation is not favorable for the reaction process.

The thermal rate constants for the two reaction channels as a function of temperature over the range of 400 K to 10000 K which are calculated within the centrifugal sudden approximation and Coriolis coupling are shown in Figure 10. It can be seen that the thermal rate constant for the channel 1 is larger than those of the channel 2. This is accord with the cross section results in Figures 4 and Figure 5. Compare with the CC and CS calculations in the two reaction channels, we can see that the CS result is lower than the CC one. The difference between the CC and CS calculations is reductive with the increase of the temperature in the channel 1 and the inverse variation is exhibited in the channel 2.

Through comparing with the CC and CS calculations for the integral cross section, we see that CC results are larger than the CS calculations. The difference between the CC and CS calculations is clearly decreasing with increasing collision energy in the LiH depletion channel and increasing in the H-exchange channel. The resonance oscillations in the reaction probability and cross section curves tend to become broader on inclusion of the CC terms. Form the Ref,[34] the Coriolis coupling effect is more pronounced under a complex-forming mechanism than a direct abstraction mechanism. In our subsequent work, the title reaction mainly goes on under an insertion mechanism based on the investigation of a mountain of quasi-classical trajectories. There is competition between the two reaction channels. Especially, when the collision is small, the competition between the two channels become strongly.

Conclusion

In this work, we performed the reaction probability and the integral reaction cross section calculations with quantum wave packet methods for the two reaction channels of H + LiH $\rightarrow$ Li + H_2 and H_b + LiH_a $\rightarrow$ LiH_b + H_a based on PMM PES. To investigate the Coriolis coupling effect in the dynamic calculation, the Coriolis coupling and centrifugal sudden approximation are carried out, respectively. In the LiH depletion channel, the CC result is larger than the CS result, and the difference tends to diminish at high collision energy. The tendency of difference between the CC and CS increases with increasing collision energy. The high rotational excitation is not favorable for the reaction process. The difference between the CC and CS rate constant calculations is reductive with the increase of the temperature in the LiH depletion channel and the inverse variation is exhibited in the H-exchange channel. There is competition between the two reaction channels. The Coriolis coupling effect in the H-exchange channel is more effectively than that in the LiH depletion channel. The high vibrational excited reagent leads the reaction to trend towards the H-exchange reaction channel.

Acknowledgments. This work is supported by the National Natural science Foundation of China (Grant No. 10874064), the Innovation Scientists and Technicians Troop Construction Projects of Henan Province (Grant No. 124200510013) and Sponsored by Program for Science (Technology Innovation Talents in Universities of Henan Province (Grant No. 13IRTSTHN016). And the publication cost of this paper was supported by the Korean Chemical Society.

References

1. Lepp, S.; Shull, J. M. *Astrophys. J.* **1984**, *280*, 465.
2. Lepp, S.; Stancil, P. C.; Dalgarno, A. *J. Phys. B* **2002**, *35*, 57.
3. Stancil, P. C.; Lepp, S.; Dalgarno, A. *Astrophys. J.* **1996**, *458*, 401.
4. Bodo, E.; Gianturco, F. A.; Martinazzo, R. *Phys. Rep. Rev. Sec. Phys. Lett.* **2003**, *384*, 85.
5. Dubrovich, V. K. *Astron. Lett.* **1993**, *19*, 53.
6. Signore, M.; Vedrenne, G.; Debernardis, P.; Dubrovich, V.; Encrenaz, P.; Maoli, R.; Masi, S.; Mastrantonio, G.; Melchiorri, B.; Melchiorri, F.; Tanzilli, P. E. *Astrophys. J. Suppl. S* **1994**, *92*, 535.
7. Yoshida, N.; Abel, T.; Hernquist, L.; Sugiyama, N. *Astrophys. J.* **2003**, *592*, 645.
8. Prodanovic, T.; Fields, B. D. *Astrophys. J.* **2003**, *597*, 48.
9. Bililign, S.; Hattaway, B. C.; Robinson, T. L.; Jeung, G. H. *J. Chem. Phys.* **2001**, *114*, 7052.
10. Chen, J. J.; Hung, Y. M.; Liu, D. K.; Fung, H. S.; Lin, K. C. *J. Chem. Phys.* **2001**, *114*, 9395.
11. Yan, Z. C.; Babb, J. F.; Dalgarno, A.; Drake, G. W. F. *Phys. Rev. A* **1996**, *54*, 2824.
12. Hsu, S. K.; Wang, J. J.; Yu, P.; Wu, C. Y.; Luh, W. T. *J. Phys. Chem. A* **2002**, *106*, 6279.
13. Mérawa, M.; Bégué, D.; Dargelos, A. *J. Phys. Chem. A* **2003**, *107*, 9628.
14. Acocella, A.; Jones, G. A.; Zerbetto, F. *J. Phys. Chem. A* **2006**, *110*, 5164.
15. Prudente, F. V.; Marques, J. M. C.; Maniero, A. M. *Chem. Phys. Lett.* **2009**, *474*,18.

16. Clarke, N. J.; Sironi, M.; Raimondi, M.; Kumar, S.; Gianturco, F. A.; Buonomo, E.; Cooper, D. L. *Chem. Phys.* **1998**, *233*, 9.
17. Lee, H. S.; Lee, Y. S.; Jeung, G. H. *J. Phys. Chem. A* **1999**, *103*, 11080.
18. Dunne, L. J.; Murrell, J. N.; Jemmer, P. *Chem. Phys. Lett.* **2001**, *336*, 1.
19. Padmanaban, R.; Mahapatra, S. *J. Chem. Phys.* **2002**, *117*, 6469.
20. Padmanaban, R.; Mahapatra, S. *J. Chem. Phys.* **2004**, *121*, 7681.
21. Padmanaban, R.; Mahapatra, S. *J. Chem. Phys.* **2004**, *120*, 1746.
22. Kim, K. H.; Lee, Y. S.; Ishida, T.; Jeung, G. H. *J. Chem. Phys.* **2003**, *119*, 4689.
23. Martinazzo, R.; Tantardini, G. F.; Bodo, E.; Gianturco, F. A. *J. Chem. Phys.* **2003**, *119*, 11241.
24. Berriche, H. *J. Mol. Struct.* **2004**, *682*, 89.
25. Berriche, H.; Tlili, C. *J. Mol. Struct.* **2004**, *678*, 11.
26. Padmanaban, R.; Mahapatra, S. *J. Phys. Chem. A* **2006**, *110*, 6039.
27. Padmanaban, R.; Mahapatra, S. *J. Theor. Comput. Chem.* **2006**, *5*, 871.
28. Wernli, M.; Caruso, D.; Bodo, E.; Gianturco, F. A. *J. Phys. Chem. A* **2009**, *113*, 1121.
29. (a) Zhang, J. Z. H. *Theory and Application of Quantum Molecular Dynamics (World Scientific, Singapore)*; Zhang, D. H., Zhang, J. Z. H. *J. Chem. Phys*. **1994**, *101*, 1146. (b) Zhang, J. Z. H.; Dai, J. Q.; Zhu, W. *J. Phys. Chem. A* **1997**, *101*, 2746.
30. Yang, B. H.; Gao, H. T.; Han, K. L.; Zhang, J. Z. H. *J. Chem. Phys.* **2000**, *113*, 1434.
31. Xie, T. X.; Zhang, Y.; Zhao, M. Y., Han, K. L. *Phys. Chem. Chem. Phys.* **2003**, *5*, 2034.
32. Zhang, Y.; Xie, T. X.; Han, K. L.; Zhang, J. Z. H. *J. Chem. Phys.* **2003**, *119*, 12921.
33. Chu, T. S.; Zhang, Y.; Han, K. L. *Int. Rev. Phys. Chem.* **2006**, *25*, 201.
34. Chu, T. S.; Han, K. L. *Phys. Chem. Chem. Phys.* **2008**, *10*, 2431.
35. Hu, J.; Han, K. L.; He, G. Z. *Phys. Rev. Lett*. **2005**, *95*, 123001.